Available online at www.sciencedirect.com

ScienceDirect

Procedia CIRP 87 (2020) 497–502

www.elsevier.com/locate/procedia

5th CIRP CSI 2020

A physically based model of *Ti6Al4V* turning process to predict surface integrity improvements

Sergio Rinaldi[a,*], Giovanna Rotella[b], Domenico Umbrello[a], Luigino Filice[a]

[a]*Department of Mechanical, Energy and Management Engineering, University of Calabria, Rende, CS 87036, Italy*
[b]*Department of Computer Engineering, Modeling, Electronics and Systems Engineering, University of Calabria, Rende, CS 87036, Italy*

* Corresponding author. Tel.: +39 0984494637; fax: +39 0984494673. *E-mail address:* sergio.rinaldi@unical.it

Abstract

In turning processes, surface improvements are strictly related to the physical phenomena induced by the involved thermo-mechanical loads. These phenomena are difficult to be analyzed while they occur, therefore the process simulation is a very important tool to deeply understand their evolution. Turning experiments were carried out on *Ti6Al4V* workpiece under different machining conditions. The microstructural modifications were analyzed in terms of metallurgical changes and micro-hardness. The physical mechanisms that occurred on the machined surface were investigated to construct a constitutive material flow model. The developed material model was implemented via sub-routine in a commercial FE software and validated through comparisons with experimental data (cutting forces, temperatures and microstructural modifications). The model was employed to predict the process variables of scientific interest (microstructural changes and surface improvement). The numerical results in main cutting forces, feed forces and temperatures prediction proved the accuracy and reliability of the proposed numerical model showing a good agreement with the experimental data.

Keywords: Physics based modeling, *Ti6Al4V*, Hard turning

1. Introduction

In polycrystalline materials, the microstructure strongly affects their mechanical properties, such as strength, ductility, creep resistance and fatigue life. Consequently, for industries, microstructure control and optimization is one of the most important issues to enhance the final product characteristics [1].

In aeronautic and aerospace industry, where final products require strong reliability, repeatability and, in general, superior mechanical properties in operating conditions, stands out the *Ti6Al4V* titanium alloy. This latter shows interesting thermomechanical properties, such as specific strength, toughness and corrosion resistance, that ease a large application in the manufacturing of artefacts that operate under particularly critical thermo-mechanical cyclic loads, such as the rotating parts of the jet turbines [2].

On the other side, *Ti6Al4V* is considered a difficult-to-cut material, because of its high-temperature strength and strong chemical affinity with the most common cutting tool materials. Therefore, in order to make possible the best employment of *Ti6Al4V* products under such critical conditions, optimization procedures of machining process parameters are needed to facilitate the processing of the alloy [3].

A process variables optimization can be carried out computing also the component surface. This latter can be controlled through a correct managing of the working parameters and lead to a product of superior mechanical characteristics.

Kadam et al. noticed that an appropriate lay out of the cutting conditions, design of the cutting tool and process parameters of *Ti6Al4V* finishing processes can lead to the production of higher performances artefacts [4]. Umbrello and Rotella

10.1016/j.procir.2020.02.017

relieved a substantial improvement in *Ti6Al4V* components fatigue toughness can be reached opportunely choosing the machining conditions [5].

Moreover, Liang et al. found that significant enhancement on both micro-hardness and residual stress status beneath the *Ti6Al4V* machined parts surface can be obtained exploiting an appropriate choice of the cutting conditions [6].

Consequently, according with the literature findings, a deep knowledge concerning the material microstructural evolution during the machining process is of fundamental importance to properly design a final product that can show the best of its potential performances [7].

In this context, Finite Element (FE) numerical modeling represents an important tool to understand the behavior of the workpiece material when it is machined, allowing to examine the material behavior at higher deformation speed than com4mon experimental procedures, such as Digital Image Correlation (DIC), permit to analyze [8].

Once numerical FE simulation is coupled with a physics based modeling of the flow stress, is possible to perform a deep examination of the microstructural phenomena occurring during material processing, allowing to predict the main variables of industrial interest and the metallurgical improvements that arise on the machined surface [9].

This paper presents a customized physics based numerical model able to describe the main microstructural modifications occurring during *Ti6Al4V* large deformation processes. In particular, the model is applied to hard turning process and the stress modeling is based on the phenomena of dislocation accumulation, dynamic recrystallization (DRX), lattice friction stress and dislocation drag effect. The model was validated with experimental results in terms of forces and temperatures and is able to correctly predict grain refinement and hardness enhancement on the machined surface and sub-surface.

2. Materials and Methods

Turning tests were conducted on *Ti6Al4V* bars with a diameter of 10 mm (382 $HV_{0.01}$) at fixed feed rate and depth of cut of 0.15 mm/rev and 0.05 mm respectively. The tests were conducted on a Mazak® Quick Turn Nexus 220-II CNC lathe at varying cutting speed (30, 50 and 70 m/min) in dry conditions.

Coated Coro Cut N123H2-0400-RO 1105 PVD TiAlN insert with a clearance angle of 7° and a rake angle of 12°. The insert cutting edge radius is 15 μm, was measured using a no contact 3D confocal profilometer. The rake face was flat oriented in the tool holder (Sandvik RF123H25-2525BM) that was fixed to a Kistler 9257 three component piezoelectric dynamometer in order to monitor the evolution of the cutting forces during the process permitting to obtain the steady state mean values for the subsequent analysis. Furthermore, a thermocouple (K-type) was embedded into the tool-holder and the tool interface to measure the local temperature at the cutting tool back during machining. This temperature was used to determine the temperature at the interface between the cutting tool edge and the machined surface by an inverse numerical methodology as done in [9].

Coupled with the described methodology, the cutting temperatures at the tool-workpiece interface were also investigated employing a IR thermo-camera in order to get information not only at the tool-workpiece interface, but also concerning the areas around it.

The experimental set up and the temperature measurement instruments details are visible in Fig. 1.

The cutting temperature taken as reference for the experimental analysis and the numerical model validation is the maximum one developed on the workpiece into the shown reference area.

The machined surfaces of each experimental test investigated were cut out from the samples and mounted into a resin holder for microstructural analysis and hardness measurements. The samples were mechanically polished and etched using Kroll's reagent (92 ml of distilled water, 6 ml of nitric acid, 2 ml of hydrocloridric acid).

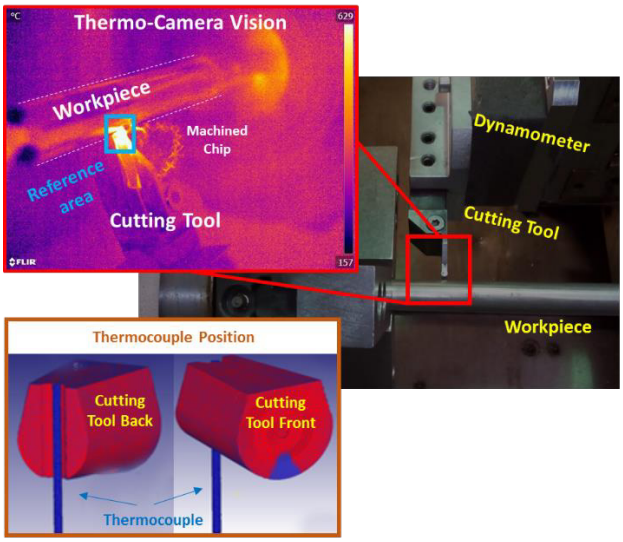

Fig. 1. Experimental setup and temperature measurement instrument details.

The microstructure was analyzed by means of an optical microscope LEICA DFC 320 (1000x of magnification), while the micro-hardness ($HV_{0.01}$) was measured on polished samples by means of a QNES10 micro-indenter using 10 s of holding time. More details regarding the experimental tests are available in a previous work [5].

3. Finite Element Model

A Finite Element model of the machining process was developed using the commercial software SFTC Deform®. A 3D thermo-mechanical multiphysics analysis was performed via Update-Lagrangian code coupled with remeshing technique in order to permit a better prediction of the large deformations that involve geometrical evolution on the processed material during the machining operations.

FE 3D modeling was based on the assumptions of a rigid machining tool (meshed into 100000 elements), while the workpiece was modelled as plastic and divided into 200000 tetrahedral elements. The mesh density was increased at the workpiece-tool edge interface area, with a mean element size of 7 μm.

The machining process has been modeled by setting up a fixed workpiece and a moving cutting tool.

The workpiece-tool thermal interaction was taken into account by setting the global heat transfer coefficient of h_{int}=10^5 kW/(m^{2}K) at the interface as suggested by the specific scientific literature [10]. The contact behavior at the interface was modeled via hybrid friction model that allows to properly simulate both sticking and sliding phenomena at the tool-workpiece interface [9]. The friction coefficients m and μ were chosen as 1 and 0.7 respectively since a "Trial and Error" calibration procedure. This procedure was carried out until the error obtained comparing the numerical predicted variables with the experimental results was minimized in a general good agreement with the experimental results.

The overall details about the setting of the numerical model and the assignment of the boundary conditions are visible in Fig. 2.

A physics based constitutive model, was employed to describe *Ti6Al4V* plastic flow stress behavior, in such way it was possible to take into account the inner phenomena occurring during the machining process.

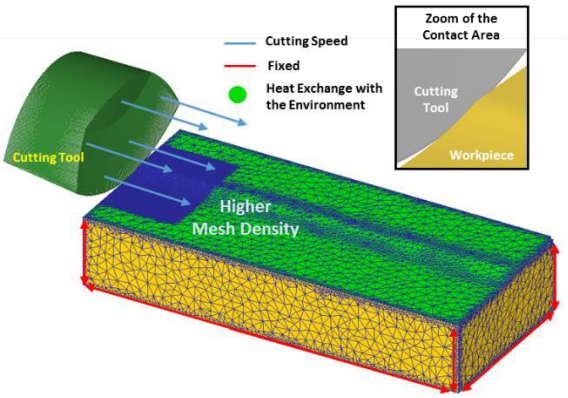

Fig. 2. Movement setup, thermal boundary conditions and contact area.

The model represents a description of the plastic stress (σ_{pl}) as algebraic sum of different terms and each one describes the contribution to the material plasticity of the main microstructural phenomena that cause stress strengthening or softening and occur during general materials large strain deformation processes (Equation 1).

$$\sigma_{pl} = \sigma_{th} + \sigma_{HP} + \sigma_G + \sigma_d \tag{1}$$

Where σ_{th} represents the *Peierls* stress, that models the resistance of the material to plastic deformation where thermal activated mechanisms support the applied stress in moving dislocations through the lattice.

σ_{HP} is the *Hall-Petch* stress and indicates the contribution of the grain size to the plastic flow and depends on the mean grain diameter, while σ_G designates the strain hardening phenomena due to the generation and accumulation of dislocations.

Finally, σ_d represents the material strengthening due to the nano-scale phenomenon of the dislocation drag.

The interaction between the mobile and immobile dislocations is the physical basis of the strengthening of a general metal material and is usually described by the well-known Taylor equation (Equation 2).

$$\sigma_G = \alpha_G M G b \sqrt{\rho_i} \tag{2}$$

Where α_G is a proportional constant, M is the Taylor factor, ρ_i is the density of immobile dislocations, G is shear modulus and b is the Burger's vector [11].

The evolution of the dislocation density is described by the two terms of Equation 3. In detail, $\rho_i^{(+)}$ represents the material strengthening due to the accumulation of dislocation nucleating during the large deformation process, while $\rho_i^{(-)}$ represents the material softening due to the grain recovery effects [12].

$$\dot{\rho}_i = \dot{\rho}_i^{(+)} - \dot{\rho}_i^{(-)} \tag{3}$$

The motion of the dislocation can be obstructed by the presence of lattice obstacles causing a strengthening effect in the material flow stress. This phenomenon is described by Equation 4 [12].

$$\dot{\rho}_i^{(+)} = \left(\frac{1}{s} + \frac{1}{D}\right)\left(\frac{M}{b}\right)\dot{\bar{\varepsilon}}^p \tag{4}$$

Where $\dot{\bar{\varepsilon}}^p$ is the equivalent plastic strain rate, D is the initial grain size and s is the crystal cell size and its evolution is described by Equation 5 [12].

$$s = K_c/\sqrt{\rho_i} \tag{5}$$

Where K_c is a calibration constant [12].

The material softening due to the recovery effect is described by Equation 6.

$$\dot{\rho}_i^{(-)} = \Omega \rho_i \dot{\bar{\varepsilon}}^p \tag{6}$$

Where Ω is the recovery function [12].

The σ_{th} term represents the material resistance to plastic deformation due to the short-range interactions where thermal activated mechanisms assist the applied stress in moving dislocations and is described by Equation 9.

$$\sigma_{th} = \tau_0 G \left(1 - \left(\frac{k_b T}{\Delta f_0 G b^3} ln\left(\frac{\dot{\varepsilon}_{ref}}{\dot{\varepsilon}^p}\right)\right)^{1/q}\right)^{1/p} \tag{9}$$

Where τ_0 is the frictional shear stress, Δf_0, q and p are calibration parameter, k_b is the Boltzmann constant (1.38064852e-23 $m^2kg/(s^2\ K)$), T is the absolute temperature and $\dot{\varepsilon}_{ref}$ is a reference strain rate typically taken as 10^6 [12].

The mean grain size D was predicted considering the common mixture law in order to take into account the contribution of both the grain structures previously existing into the material and the fraction of new grains generated by the dynamic recrystallization phenomenon (Equation 10):

$$D = D_{DRX} X_{DRX} + D_0(1 - X_{DRX}) \tag{10}$$

Where D_0 is the average initial grain size ($5\ \mu m$), D_{DRX} is the dynamically recrystallized grain size (Equation 11) and X_{DRX} is the volume fraction of the recrystallized grains, this latter is described by the Avrami model (Equation 12) [13, 14].

$$D_{DRX} = 1.847Z^{-0.13} \tag{11}$$

$$X_{DRX} = 1 - exp\left(-0.9339\left(\frac{\varepsilon-\varepsilon_{cr}}{\varepsilon_{0.5}}\right)^{0.5994}\right) \tag{12}$$

As showed by Equation 12, the volume fraction of recrystallized grains depends on material strain (ε), critical strain for the nucleation of the recrystallized grains (ε_{cr}), as described by Equation 13, $\varepsilon_{0.5}$ (Equation 14) that is the strain that refers to the 50% of recrystallized grains fraction and Z that is the Zener-Hollomon parameter that is described by Equation 15 [13, 14].

$$\varepsilon_{cr} = 0.1311 * 0.0064\dot{\varepsilon}^{0.0801} * exp\left(\frac{26430}{RT}\right) \tag{13}$$

$$\varepsilon_{05} = 0.022 * \dot{\varepsilon}^{0.11146} * exp\left(\frac{30579}{RT}\right) \tag{14}$$

$$Z = \dot{\varepsilon}^{p} exp\left(\frac{341700}{RT}\right) \tag{15}$$

The *Hall-Petch* stress (σ_{HP}) depends on the mean grain size of the investigated material and represents the contribution to the material strengthening given by the grain boundaries that tends to hinder the dislocation motion. Its expression is given by Equation 16 [11].

$$\sigma_{HP} = \alpha_{HP} G \sqrt{b/D} \tag{16}$$

Where α_{HP} is a calibration constant.

Another important phenomena occurring on the investigated material when is subjected to high strain rate large deformation is dislocation drag.

Dislocation drag is believed to be a viscous mechanism that is due to the interaction between dislocations and lattice phonons that significantly increase the material strain rate sensitivity.

The following phenomenological form (Equation 17) was used by [11] to describe this specific strengthening phenomenon for *Ti6Al4V*.

$$\sigma_d = M\tau_d\left(1 - exp(-\alpha_d\dot{\varepsilon}^{p})\right) \tag{17}$$

The value of the constant used in the proposed model obtained by literature analysis [11-14] are reported in Table 1.

In order to confirm the compatibility of the proposed flow stress model with the material used for the experimental tests a comparison with experimental tensile tests was carried out showing a good match (R^2 higher than 90%).

Table 1. Numerical constants.

Numerical Constant	Value	Numerical Constant	Value
b [m]	2.95e-10	τ_0	0.02
α_G	1.9	Δf_0	0.5
M	3.07	p	0.3
ρ_0 [m^{-2}]	1e14	q	1.8
K_C	40	α_{HP}	0.413
Ω	38	$M^*\tau_d$	225
K_c	36	α_d	0.001

4. Results and Discussion

4.1. Machining forces and temperatures

Fig. 3 reports a comparison between both the numerical predicted cutting forces and temperatures and the experimentally obtained ones.

The predicted main cutting forces are in good agreement with those that were measured during the experimental procedures, with an overall average absolute error of nearly 5%. The thrust forces obtained from the model showed a mean absolute error equal to 4.04%, while the feed forces comparison showed an error of 12.93%. Concerning the cutting temperatures prediction, an average absolute error of around 7% is noticeable.

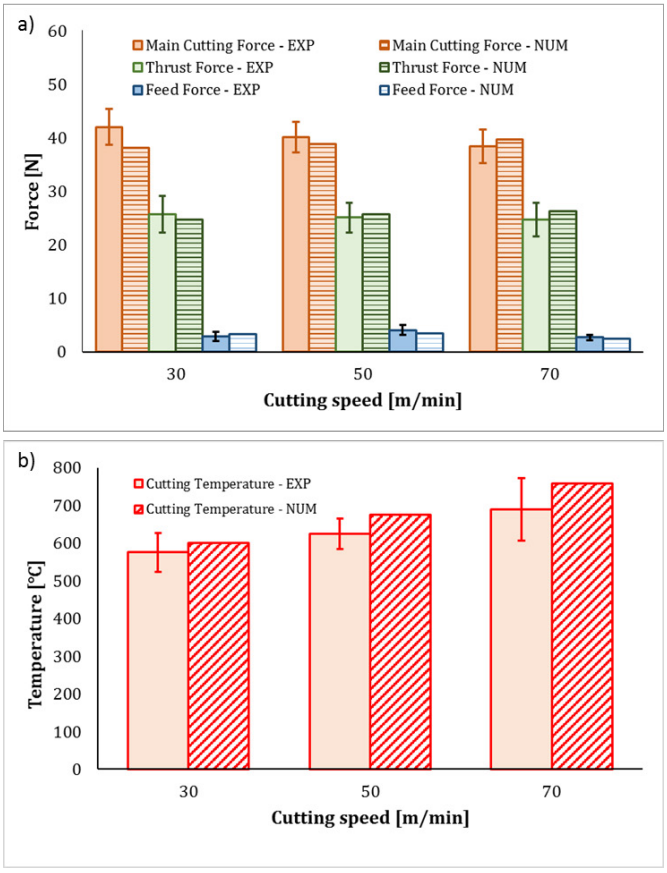

Fig. 3. Mean and variation of experimental (EXP) and numerical simulated (NUM) cutting forces, thrust forces and feed forces (a) and temperatures (b).

The two latter mean errors are higher than the ones on the main cutting forces and thrust forces. However, due to the huge nonlinearity involved into the deformation process simulated, the unavoidable physical limits of the hybrid friction model and the interpolation error due to the updating of the geometry because of the remeshing technique employed to simulate the large deformation conditions, this specific entity of error was considered acceptable. Moreover, it is important to point out that, during machining of hard materials, the tool geometry unavoidably changes, due to the wear effect. This aspect was not modelled because of the too high computational cost involved, therefore the higher error in feed forces was also attributed to the absence of tool wear in the numerical model that introduces significant non-linearity in the friction and contact modeling, which are unavoidably present in the machining of superalloys [9]. On the other hand, in order to contain this unavoidable phenomenon as much as possible a fresh tool was used for each case study during the experimental procedures and the tool wear was monitored at the end of each test to be as slight as possible.

4.2. Surface integrity

Depending on the machining parameters, different phenomena may occur on the worked surface and sub-surface.

Zones of intense slip activity behave as preferred site for grains nucleation, causing DRX. In detail, grain refinement layers were noticed on the machined surfaces, where the thermo-mechanical loads were more prominent.

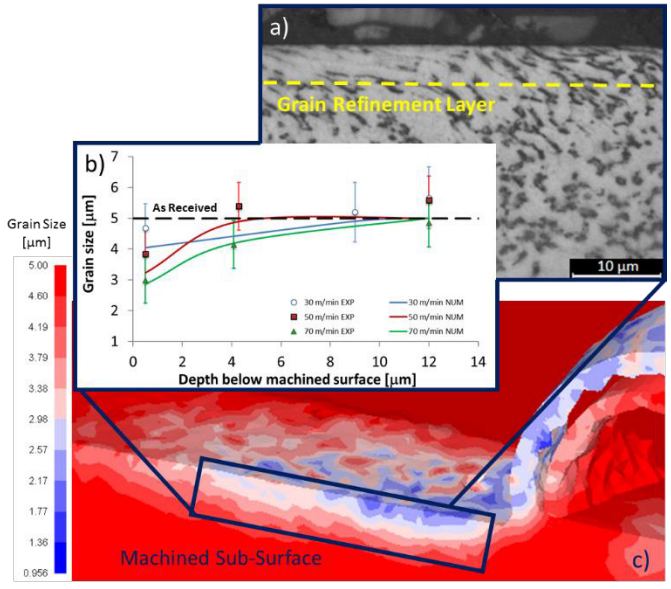

Fig. 4. Microstructure (a), comparison between numerically predicted and measured grain size (b) and grain size distribution in FE model (c) at 50 m/min.

In detail, the thicknesses of these layers are lower than 8 µm for each investigated case and the dimensions of the layers are always comparable with the numerical predicted ones (Fig. 4a and 4c).

Fig. 4b shows the comparison between the numerical and the experimental distribution of grain size measured on the machined subsurface and along the depth. In particular, the grain refinement is more significant when the cutting speed is higher because of the higher quantity of deformation and thermal energy imposed by severer machining conditions that cause a significant increment of the plastic work at the tool-workpiece interface.

A physics based numerical model generally represents an extremely useful tool able to deeply investigate the crystalline phenomenon due to the thermo-mechanical loads imposed on the metals. Consequently, the FE simulation was used to predict with excellent approximation the grain size changes phenomena induced by the machining process.

Moreover, referring to Fig. 5 is possible to observe that the fraction of recrystallized grains (X_{DRX}) is predominant on the machined surface and extremely beneath it. Consequently, taking into account that dynamically recrystallized grains grow poor of dislocations [13], the main contribution in micro-hardness increasing was attributed to the grain refinement effect.

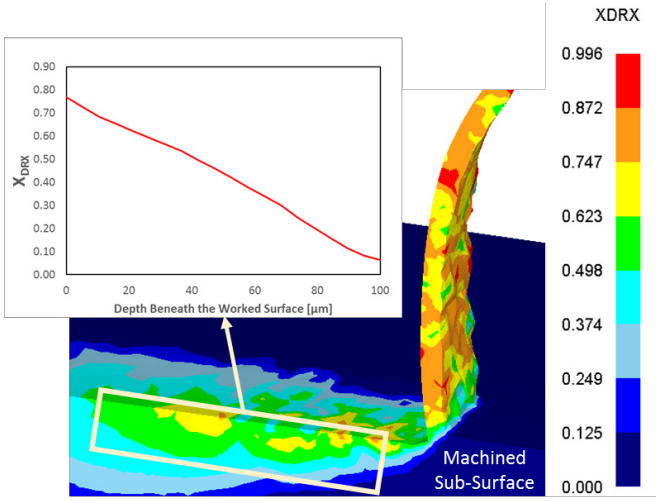

Fig. 5. Volume fraction of recrystallized grain size (X_{DRX}) beneath the machined surface (30 m/min).

Therefore, the *Hall-Petch* hardening prediction model (Equation 18) was used to predict the increment of micro-hardness on the worked surface and all along the affected layer [9].

$$HV = C_0 + \frac{C_1}{\sqrt{D}} \tag{18}$$

Where C_0 and C_1 are calibration constants and their values were calibrated via "*Trial and Error*" procedure and set as 209 and 393 respectively .

According with the experimental results, it is possible to notice that a hardened layer of around *50 µm* of thickness is present beneath the machined surface in all the investigated case studies. A slight increment of hardness is visible with the increasing of the cutting speed, according with the slight increment of grain refinement rate previously discussed (Fig. 4).

The comparison between the measured and the predicted micro-hardness is reported in Fig. 6.

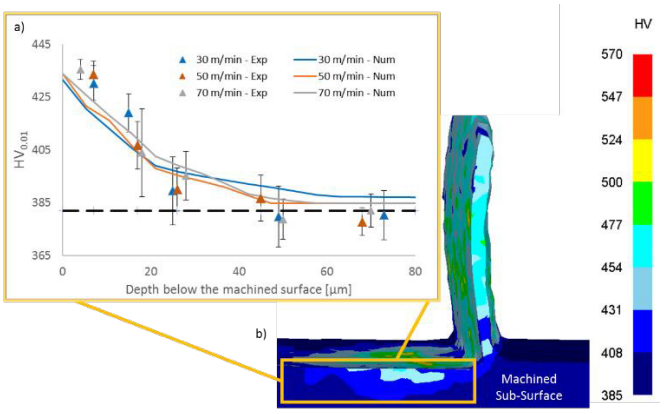

Fig. 6. Comparison between the measured and numerical predicted surface and sub-surface micro-hardness (a) and hardness distribution in FE model (b) at 70 m/min.

The hardness prediction given from the numerical model shows a good match with the experimental results corroborating the goodness of the model and confirming its effectiveness as a convenient tool able to investigate and predict the metallurgical changes that occur when the investigated alloy is subjected to severe mechanical deformations.

5. Conclusions

In this work the machining behavior of Ti6Al4V was investigated using a physically based finite element constitutive model in order to explore the main metallurgical phenomena that occur during machining with particular regard to dynamic recrystallization.

The dynamic interaction between mobile and immobile dislocations are taken into account in order to understand the plastic flow behavior when plastic deformation is induced by the machining tool. Moreover, the hardness modification was also implemented into the FE model in order to understand its distribution beneath the machined surface, when different cutting speed are used.

The affordability of the proposed model was verified through the comparison between numerical and experimental results. The numerical data were in good agreement with the experimental ones. The average total error between the predicted and the measured main cutting forces and thrust forces was not higher than 5%, while the mean absolute error on feed force and cutting temperature prediction was of around 13% and 7% respectively.

Through the FE simulation, it was possible to predict also the layer beneath the machined surface hardened by the turning process. According with the numerical model predictions, the hardening effect was attributed to the grain refinement phenomenon and modeled using the *Hall-Petch* law, showing a good agreement with the micro-hardness measured on the processed surface.

The employment of a physics based model allows to get a deeper understanding of the metallurgical phenomena occurring when large plastic strains are involved with a better prediction of the experimental data, that is a fundamental standing in the design of high performance and reliable industrial processes.

References

[1] R Ding, ZX Guo. Microstructural evolution of a Ti–6Al–4V alloy during β-phase processing: experimental and simulative investigations. Materials Science and Engineering A 365; 2004. p. 172–179.

[2] B Babu, LE Lindgren. Dislocation density based model for plastic deformation and globularization of Ti-6Al-4V. International Journal of Plasticity 50; 2013. p. 94-108.

[3] G Rotella, S Rinaldi, L Filice. Roller burnishing of Ti6Al4V under different cooling/lubrication conditions and tool design: effects on surface integrity. The International Journal of Advanced Manufacturing Technology; 2019. P 1-10.

[4] GS Kadam, RS Pawade. Surface integrity and sustainability assessment in high-speedmachining of Inconel 718eAn eco-friendly green approach. Journal of Cleaner Production 147, 2017. p. 273-283.

[5] D Umbrello, G Rotella. Fatigue life of machined Ti6Al4V alloy under different cooling conditions. CIRP Annals 67; 2018. p. 99-102.

[6] X Liang, Z Liu, W Liu, B Wang, GYao. Surface integrity analysis for high-pressure jet assisted machined Ti-6Al-4V considering cooling pressures and injection positions. Journal of Manufacturing Processes 40, 2019. p. 149-159

[7] T Sekiguchi, K Ono, H Fujiwara, K Ameyama. New Microstructure Design for Commercially Pure Titanium with Outstanding Mechanical Properties by Mechanical Milling and Hot Roll Sintering. Materials Transactions 51; 2010. p 39-45.

[8] D Zhang, XM Zhang, WJ Xu, H Ding. Stress Field Analysis in Orthogonal Cutting Process Using Digital Image Correlation Technique. Journal of Manufacturing Science and Engineering 139; 2017.

[9] S Imbrogno, S Rinaldi, D Umbrello, L Filice, R Franchi, A Del Prete. A physically based constitutive model for predicting the surface integrity in machining of Waspaloy. Materials & Design 152; 2018. p 140-155.

[10] D Umbrello, A Bordin, S Imbrogno, S Bruschi. 3D finite element modelling of surface modification in dry and cryogenic machining of EBM Ti6Al4V alloy. CIRP Journal of Manufacturing Science and Technology 18; 2017. p. 92-100.

[11] P Fernandez-Zelaia, S Melkote, Troy Marusic, S Usui. A microstructure sensitive grain boundary sliding and slip based constitutive model for machining of Ti-6Al-4V. Mechanics of Materials 109; 2017. p. 67-81.

[12] B Babu, LE Lindgren. Dislocation density based model for plastic deformation and globularization of Ti-6Al-4V. International Journal of Plasticity 50; 2013. p. 94-108.

[13] GZ Quan, GC Luo, JT Liang, DS Wu, A Mao, Q Liu. Modeling for the dynamic recrystallization evolution of Ti-6Al4V alloy in Two phase temperature range and a wide strain rate range. Computational Material Science 97; 2015. p. 136-147.

[14] H Matsumoto, V Velay. Mesoscale modeling of dynamic recrystallization behaviour, grain size evolution, dislocation density, processing map characteristic and room temperature strength of Ti-6Al-4V alloy forged in the (α+β) region. Journal of Alloys and Compounds 708; 2017. p. 404-413..